Dam-Break Wave Propagation in Alpine Valley with HEC-RAS 2D: Experimental Cancano Test Case

Dam-break wave propagation in an alpine valley with HEC-RAS 2D: the experimental Cancano test case

Marco Pilotti Ph.D, corresponding author: marco.pilotti@unibs.it, University of Brescia, Italy
Luca Milanesi Ph.D : luca.milanesi@unibs.it, University of Brescia, Italy
Vito Bacchi Ph.D : vito.bacchi@irsn.fr, Institute for Radiological Protection and Nuclear Safety, France
Massimo Tomirotti Ph.D : massimo.tomirotti@unibs.it, University of Brescia, Italy
Andrea Maranzoni Ph.D : andrea.maranzoni@unipr.it, University of Parma, Italy

Abstract

Flood modeling by the numerical solution of the 2D shallow water equations is ordinary practice. In this direction, HEC-RAS 2D has recently been released along with a suite of test cases showing the very good performance of the code in many practical situations. However, validation test cases aimed at demonstrating the capability of the software to deal with dam-break floods on very steep and irregular bathymetries are very limited. In this paper, HEC-RAS 2D is tested against the hydrographs measured in a historical physical model built in Froude similitude to analyze the consequences of the hypothetical collapse of the Cancano I dam (northern Italy) and the propagation of the resulting dam-break wave along the 15 km reach of the downstream alpine valley. The experimental hydrographs and the measured extent of the flooded areas are well reproduced by the numerical simulations. Moreover, the results obtained with HEC-RAS 2D are in very good agreement with those obtained using TELEMAC 2D, which confirms the suitability of the former software for dam-break flood studies in steep alpine valleys. The data of the test case are made available to the scientific community for validation purposes.

Introduction

Despite the benefits provided by dams for different purposes (e.g., water supply, floods control, hydropower generation, and irrigation), floods generated by the potential collapse of these structures may have catastrophic

consequences on downstream areas. In addition, the flooding risk due to the potential dam-break of many of the older dams is growing because of downstream urban development, structural deterioration, or inadequate spillway capacity. On the other hand, the failures of important dams, such as Gleno (Italy), Malpasset (France), and Teton (Idaho, U.S.), induced several governmental agencies to enact specific prescriptions requiring dam owners to perform dam-break hazard analyses for risk assessment and mitigation (e.g. ICOLD, 1998). To this end, flooding hazard assessment provides the fundamental information to be coupled with proper vulnerability and exposure metrics for the potential targets (e.g., people, buildings, and vehicles; see Milanesi et al., 2015, 2016, 2018; Milanesi and Pilotti, 2019).

Although the flow following a dam-break is inherently three-dimensional (3D), especially in the near field, fully 3D simulations are still computationally unfeasible in most practical situations. Accordingly, the widely accepted approach for dam-break hazard analysis is based on the classic Shallow Water Equations (SWE), since they combine reasonable computational effort and adequate description of the physical phenomenon (e.g. Molinaro and Natale, 1994; ICOLD, 1998; Chaudhry, 2008). The interest of this particular field of application of SWE is demonstrated by the wide literature dealing with the peculiar numerical aspects of dam-break flow simulation, like wet/dry boundaries, transcritical flow, and shocks (e.g. Bermudez and Vazquez, 1994; Bates and Hervouet, 1999; Defina, 2000; Toro, 2001; Bradford and Sanders, 2002; Caleffi et al. 2003; Toro and Garcia Navarro, 2007; Aureli et al., 2008; Hou et al., 2013; Touma and Kanbar, 2018) and with the definition of suitable test cases for validation purposes (e.g. Fraccarollo and Toro, 1995; Soares-Frazão and Zech, 2007; Aureli et al., 2008; Pilotti et al., 2011; Martínez-Aranda et al., 2018). Many research activities on these topics have also been carried out in the framework of the European projects *CADAM* and *IMPACT* (e.g. Soares Frazão et al., 2000; 2003; Morris, 2000; 2005).

The application of 2D SWE models is currently made easier by the increasing availability of specific user-oriented computational codes. A comprehensive review of many 2D solvers capable of modeling flood inundations has been recently performed by Teng et al. (2017), and the performance of some of the most used 2D software are compared by Néelz and Pender (2013). HEC-RAS 2D (Brunner, 2016) and TELEMAC 2D (TELEMAC Modelling System, 2011) are freely distributed software used in this paper due to their wide diffusion in research and practice for river system modeling. While the use of TELEMAC 2D in dam-break analyses in the presence of real topography is well documented in the literature (e.g. Hervouet and Petitjean,

1999; TELEMAC Modelling System, 2011; Paquier and Goutal, 2016), the use of the recently released HEC-RAS 2D for these applications is still rare and is documented for only few dam-break test cases (Brunner, 2018a; 2018b), including the well-known Malpasset dam-break event, already widely employed for the validation of SWE numerical models (e.g., Valiani et al., 2002; Erpicum et al., 2004; Pianese and Barbiero, 2004; Savant et al., 2011; Robb and Vasquez, 2015). Even if the use of HEC-RAS 2D is still sporadic (e.g., Quirogaa et al., 2016; Afshari et al., 2018; D'Oria et al., 2019; Shustikova et al., 2019), this software is very likely going to become a standard in free surface flow modeling, as for its well-known 1D counterpart.

In the presence of real bathymetries characterized by steep slopes, the shallow water assumptions of small bed slopes and negligible vertical accelerations (e.g. Cunge et al. 1980; Chaudhry, 2008) can be violated in several parts of the computational domain. The effectiveness of SWE under these conditions is still an interesting issue, especially in the context of dam-break analyses, since reservoirs are often placed in mountain environments (e.g. Pilotti et al., 2010, 2011).

The validation of numerical codes is typically based on analytical solutions, laboratory experiments, and available real-field data concerning historical events. Analytical solutions, usually characterized by simple geometries and mostly by frictionless bottom (e.g. Ritter, 1892; Stoker, 1948; Su and Barnes, 1970; Thacker, 1981; MacDonald et al., 1997; Delestre et al., 2013), are valuable tools to verify the performance of the numerical schemes in dealing with specific issues, but do not provide any information about the validity of the underlying mathematical model in describing the actual physical phenomenon. Such information can be obtained from laboratory experiments, even if possible scale effects must be carefully considered in transferring the results from the model to the real scale. Among the very few physical models based on real topographies, the best known is the one built in 1964 by Electricité de France in order to reproduce the Malpasset dam-break event (e.g., Goutal, 1999; Hervouet and Petitjean, 1999; Valiani et al., 2002). In the model maximum water depths were measured at 14 gauges. Another test case widely used in the literature is the physical model built by ENEL–HYDRO to study the propagation of a flood wave in a stretch of the Toce River (northern Italy). During the experimental investigation, water depth hydrographs were measured at 33 selected points (e.g. Soares Frazão and Testa, 1999; Brufau et al., 2002; Caleffi et al., 2003). Finally, historical real-field test cases include all the possible complexity aspects that can challenge physical and numerical models, but the available data are often incomplete and affected by higher uncertainties. However, in the

presence of an adequate level of documented detail, they can be used to assess the capability of the models to reproduce the most important aspects needed in flood hazard analysis (i.e., maximum water depths and velocities, flood extent, arrival time of the flood wave at specific locations). Examples of case studies analyzed in the literature are the well-known catastrophic dam-break events of Lawn Lake (Jarrett and Costa, 1986), Malpasset (Goutal, 1999), Tous (Alcrudo and Mulet, 2007), St. Francis (Begnudelli and Sanders, 2007), Gleno (Pilotti et al. 2011), and Sella Zerbino (Petaccia et al., 2016).

In a seminal work published in the Italian journal "L'Energia Elettrica", De Marchi (1945) coupled experimental (on a physical model) and simplified numerical analyses to study the propagation of the flood wave caused by the hypothetical collapse of the Cancano I dam along the Adda River (northern Italy). Physical modeling was used to overcome the difficulties related to the mathematical modeling in the upper portion of the valley characterized by very steep and irregular topography, and the experimental results were used as upstream boundary condition for the mathematical model in the downstream part of the valley. More recently, the same strategy was used, for instance, by Chaudhry et al. (1983) to analyze the generation and propagation of waves created by a hypothetical landslide in a reservoir.

The Cancano test case is very interesting for the validation of numerical models of dam-break flows because experimental discharge hydrographs are available at three different cross-sections of the model, namely immediately downstream of the dam, at the entrance to the floodplain (central portion of the physical model), and at the end of the model. This kind of data, not usually available in similar test cases, can be used as upstream boundary conditions or as benchmarks for the validation of mathematical models. Moreover, the upper stretch of the physical model is characterized by very steep slopes, both in longitudinal and transverse directions of the valley. Conversely, the downstream stretch has milder slopes, which are compatible with the classic shallow water hypothesis of small bottom slopes.

A preliminary reconstruction of the Cancano test case was presented by the authors in a previous paper (Pilotti et al., 2014), focused on the comparison between the experimental data and the numerical results obtained with a 1D SWE numerical model and a 2D SWE commercial code. The current paper upgrades the previous research by providing to the scientific community a critically revised complete data set of the Cancano dam-break test case, including a careful reconstruction of the bathymetry of the physical model. In addition, this paper provides first detailed analysis of the capability of HEC-RAS 2D to predict dam-break flow propagations in

mountain areas characterized by very steep and irregular bathymetries. Although the validation report of HEC-RAS 2D presents the application of the software to the Malpasset dam-break test case (Brunner, 2018b), where only few data on the arrival time of the flood wave and on the maximum water depths at selected locations are available, the Cancano test case allows to widen the analysis due to the unique availability of experimental discharge hydrographs at three different cross-sections. Finally, with respect to the previously published research, this paper makes a comparative use of freeware flood propagation models (HEC-RAS 2D and TELEMAC 2D) for a more comprehensive analysis of the dam-break test case.

The Cancano test case

The reinforced concrete arched gravity Cancano I dam (Fig. 1a) was built in 1924 in the upper reach of the Adda valley (Valtellina, northern Italy) for hydropower purposes. The dam had a maximum height of 60 m (with the crest located at 1859.5 m a.s.l.), a length at the top of approximately 265 m, and a storage of approximately $24 \cdot 10^6$ m^3. In 1953, the new higher Cancano II dam (yellow line in Fig. 1b) was built just downstream of the Cancano I dam (blue line in Fig. 1b) in order to increase the reservoir storage capacity to $123 \cdot 10^6$ m^3. Accordingly, the Cancano I dam is now totally submerged in the reservoir created by the Cancano II dam.

In 1943, after the attacks to the Möhne and Edersee dams during World War II, which caused catastrophic floodings in Germany, also the Cancano I dam was regarded as a potential military target. Therefore, De Marchi was asked to study the effects of a possible collapse of this dam. The analysis was limited to the upper portion of the valley, from the dam up to the village of Tirano (Fig. 2a), and the results were summarized in a paper (De Marchi, 1945; see supplementary file S2) that is an early and exceptional example of coupling of experimental and numerical techniques to investigate dam-break flood hazard in mountain areas.

The 8 km Adda River reach from the Cancano I dam to Section 23 (Fig. 2a) is very irregular and steep (the mean bed slope is 7.5%), with long stretches characterized by bed slopes greater than 20%. The valley is more regular and less steep from Section 23 to Cepina, where the mean bed slope is approximately 1% (Fig. 2b). The virtual flight above the valley provided in the supplementary materials of this paper (File S3) gives an idea of the characteristics of this stretch. Due to these peculiar geometric features and the computational resources available in 1945, De Marchi studied the upper part of the valley (from the dam to Cepina) with a 1:500 scaled physical model in Froude similitude (Fig. 3),

141 and the downstream portion of the valley (from Cepina to Tirano; Fig. 2a) with a simplified numerical model. He
142 considered two different scenarios of total and partial collapse (reproduced by the sudden removal of a plate
143 representing the dam) starting from a dry bed condition.
144 The bathymetry of the valley, including the portion of the reservoir close to the dam, was reproduced in the physical
145 model through a sequence of cross-sections connected by a cement surface (Fig. 3b). The volume of the reservoir was
146 reproduced exactly. The cross-sections were probably obtained by available maps and field surveys, and presumably
147 were not characterized by a high level of geometric detail because the lateral steepness of the valley between the dam
148 and Section 23 did not allow a good cartographic representation in the historical maps. Unfortunately, no information
149 is remained about these cross-sections and only the location of the cross-sections between Section 23 and Cepina,
150 spaced 300 m apart on average (Fig. 4), was shown in a figure of the original paper. Nowadays, an accurate
151 representation of the valley topography can be obtained by using a digital terrain model (DTM) with a 5 m resolution.
152 The discharge hydrographs for both the partial and total collapse scenarios were measured in the physical model at the
153 three cross-sections shown with red dots in Fig. 3a, namely just downstream of the dam, at Section 23, and at Cepina.
154 To this end, a slot was alternately opened on the bottom of the model at these cross-sections, and the falling water was
155 collected in a calibrated tank. The water level rise in this tank was carefully measured by using a floating recording
156 device, visible on the left of Fig. 3b. In this regard, De Marchi (1945) found that a vertical excursion of the floating
157 device of 0.002 m s^{-1} corresponded to a discharge of 5600 m^3 s^{-1}. Then, graphic operations on the recorded filling time
158 series provided the discharge hydrographs (Fig. 5). Several runs were performed in the same test conditions to verify
159 the repeatability of the physical process and the consistency of the measuring procedure. The final hydrographs of each
160 scenario were obtained by averaging the corresponding set of measures. Table 1 summarizes the peak discharges Q_p
161 (m^3 s^{-1}) and the arrival times t_a (s) of the dam-break waves measured at the three control sections for both the scenarios
162 of total and partial collapse. It is worth noting that, as a term of comparison, the peak discharge of the 100 year return
163 period natural flood at the section of Cepina is in the order of 500 m^3 s^{-1}.
164 De Marchi used the hydrographs measured at Section 23 and at Cepina to calibrate a simplified numerical model based
165 on the kinematic wave equation, which was solved using a classic level pool routing procedure by a finite difference
166 method. The discharge hydrograph measured at Cepina was propagated along the downstream 32 km river reach as
167 far as Tirano (Fig. 2a) using this numerical model. This stretch of the valley was described by means of 58 cross-
168 sections.

All the relevant data recovered from the original report by De Marchi (i.e., measured hydrographs, locations of the cross sections, and flooded areas), along with the bathymetry reconstructed for the present study, are provided as supplementary material of this paper.

As mentioned in the previous section, the information regarding the original bathymetry of the physical model is not available. On the other hand, a faithful reproduction of the valley topography between the dam and Cepina is provided by the current DTM, from which a DTM with 60 m grid size (in the following mentioned as DTM_60) was easily computed. This spatial resolution was selected because it is deemed comparable to the one of the De Marchi's cross-sections, which were described by a limited number of points, as shown in the original paper (see Fig. 14 at page 336 of De Marchi's paper in the supplementary material).

Actually, the only information available regarding the bathymetry of the physical model is the position of the cross-sections used to reproduce the valley between Section 23 and Cepina, which is shown in the original paper (Fig. 4). Therefore, a bathymetry closely reproducing the physical model can be reconstructed only for this stretch of the valley. To this purpose, cross-sections matching the position of those shown in the original paper were extracted from DTM_60 and were linearly interpolated in order to reproduce the connecting surface, mimicking the construction process of the physical model. In the following, the related DTM is named as DTM_Sect23_Cepina. On the other hand, the location of the cross-sections used to build the physical model between the dam and Section 23 is unknown. Hence, it is not certain that a bathymetry based on DTM_60 reproduces the topography originally used by De Marchi, which was probably extracted from 1910-1930 historical maps, very poor of details in the steepest part of the valley. Accordingly, on the basis of these considerations, we believe that a reliable reconstruction of the physical model topography is possible only in the stretch between Section 23 and Cepina .

A preliminary analysis was done to assess the potential influence of scale effects on the measures performed on the experimental model. Chanson (2004) states that in river models built according to the Froude similitude, viscous effects are negligible if $R > 5000$, where R is the Reynolds number. A possibly sounder condition commonly accepted in literature as a practical criterion for fully rough turbulent flow in open channels is based on the friction Reynolds number $R^* > 70$ (e.g., Yalin, 1977) or $R^* > 100$ (e.g., Henderson, 1966), where $R^* = \varepsilon u^*/\nu$, u^* is the shear velocity, ε is the scale length of the roughness, and ν is the kinematic viscosity. In order to check the fulfillment of these requirements in the physical model, the following procedure was applied. Using the method proposed by Pilotti

(2016), the geometric properties and the 1D normal depth stage-discharge relationships were computed for approximately 600 cross-sections extracted from DTM_Sect23_Cepina. On the basis of these relations, R and R* were computed for each selected cross-section for all the discharge values in the range 0÷18500 $m^3 s^{-1}$. In particular, considering the characteristic values of ε for the surface roughness of cement and concrete canals (e.g., Chow, 1959; Henderson, 1966), R* was computed assuming $\varepsilon = 0.0025$ m, that is probably representative of the size of sand grains used to line the model surface and make it artificially rough, as described in De Marchi (1945). Then, the average values of both R and R* over the entire set of cross-sections were computed at the model scale for each discharge at the prototype scale (Fig. 6).

Figure 6 shows that the average Reynolds number is usually greater than 5000 in the physical model, whereas $R^* \approx 100$ only for $Q > 10000$ $m^3 s^{-1}$ on average. Since the peak discharges between Section 23 and Cepina range from 10200 to 18300 $m^3 s^{-1}$ for the total collapse scenario (Tab. 1) and from 4300 to 5700 $m^3 s^{-1}$ for the partial collapse scenario, it can be concluded that scale effects were probably significant in the partial dam-break scenario. For this reason, the presentation of the test case is only limited to the total collapse scenario between Section 23 and Cepina.

The propagation of the dam-break wave was modeled by HEC-RAS 2D, and a sensitivity analysis on the mesh size and on the roughness coefficient was performed. As detailed in the following section, the measured hydrograph at Section 23 was used as upstream boundary condition for the numerical model. The computed hydrograph at Cepina and the predicted flooded areas were compared with the experimental data by De Marchi (1945) and with the results of numerical simulations performed with TELEMAC 2D.

Although the bathymetry of the physical model between the dam and Section 23 is unknown, an elevation model of this portion of the valley (DTM_dam_Sect23) was constructed using DTM_60 in order to compare the capabilities of HEC-RAS 2D and TELEMAC 2D to deal with a dam-break over a crooked and steep domain. In this case, the discharge hydrograph measured at the dam was imposed at the upstream boundary of the computational domain. The numerical hydrographs computed at Section 23 were also compared with the experimental data.

HEC-RAS 2D model setup

The computational mesh for HEC-RAS 2D was built on the surface of the topography provided by DTM_Sect23_Cepina, creating an unstructured mesh composed of cells with up to eight sides, that far from

boundaries and internal singularities, was formed by squared elements in order to improve computational efficiency. Moreover, the mesh was built using the so-called "high resolution subgrid model" (Casulli and Stelling, 2011), which allows coarse computational meshes to be used without losing the detail of the underlying terrain (Brunner, 2016).

The physical model had a concrete lining whose Manning coefficient n reasonably lay in the range 0.014÷0.018 s $m^{-1/3}$ at the model scale (Chow, 1959), that corresponds to 0.04÷0.055 s $m^{-1/3}$ at the prototype scale. It can be noted that Testa et al. (2007) suggested n = 0.0162 s $m^{-1/3}$ for a similar laboratory concrete lined physical model at a scale of 1:100 of a reach of the Toce River valley (western Alps, Italy). Since the concrete lining of the physical model was uniform, the Manning coefficient was assumed to be homogeneous along the entire valley stretch, even if in the real valley a spatial variation depending on topography and on land use would be expected. In order to assess the effect of bottom roughness on the results, a sensitivity analysis on this parameter was performed considering three values: 0.04, 0.045, and 0.05 s $m^{-1/3}$. These values are coherent with the parameter n = 0.05 s $m^{-1/3}$ used by De Marchi (1945) for the numerical propagation of the dam-break wave in the valley stretch from Cepina to Tirano.

A discharge hydrograph can be used as inflow boundary condition in HEC-RAS 2D . An energy slope value, often assumed equal to the bed slope, is required to determine the normal depth for each discharge value. Based on the normal depth and on the conveyance of the inflow cross-section, the flow is distributed to the cells along the boundary. The experimental hydrograph measured at Section 23 for the total collapse scenario, coupled with a slope of 0.03 m/m, was imposed at the upstream inflow boundary, while a normal depth outflow boundary condition was set at Cepina. The numerical results presented in a following section, concerning the upper reach of the valley, show that the flow is mainly supercritical at Section 23, which confirms the suitability of the normal depth condition at the inflow section. In the numerical simulations, a dry initial condition was assumed in the overall domain, as in the physical model.

HEC-RAS 2D solves the 2D SWE (in the complete form or with the diffusion wave approximation) with an implicit finite volume algorithm. In this study, the full 2D SWE were adopted and a variable time step was preferred to a fixed-time step to advance the numerical solution in time. Moreover, it was verified that the model results do not change significantly when turbulence effects are included, as can be done in HEC-RAS

2D by means of a classic second-order viscous term in which an eddy viscosity coefficient appears (Brunner, 2016).

Results

In this section, the numerical predictions of HEC-RAS 2D are compared with the experimental data of the Cancano test case to assess the capabilities of HEC-RAS 2D to deal with the propagation of a dam-break wave along a mountain valley.

Using DTM_Sect23_Cepina, a sensitivity analysis on the size of the computational grid was initially performed using meshes with average cell size Δ = 60 m, 30 m, 20 m, and 15 m and a constant value of the roughness coefficient throughout the computational domain (n = 0.045 s m$^{-1/3}$) as discussed in the following. Figure 7a shows the comparison between the experimental hydrograph at Cepina and the ones computed with the different meshes. The wave arrival time and the peak discharge are almost insensitive to the average mesh size when Δ < 30 m ($t_a \cong$ 1160 s and 9910 m^3 s^{-1} < Q_p < 10110 m^3 s^{-1}), whereas Δ = 60 m provides the fastest wave (t_a = 1100 s) and the highest peak discharge (Q_p = 10657 m^3 s^{-1}). In general, the numerical discharge hydrographs obtained with Δ < 30 m are in good agreement with the experimental one and the simulations performed with Δ = 20 m and Δ = 15 m predict almost identical peak discharges at Cepina. In general, the shape of the numerical hydrographs is not significantly affected by the grid spacing. Finally, the extent of the flooded domain does not show relevant variations due to the different average cell spacing, that is largely a consequence of the application of the meshing algorithm proposed by Casulli and Stelling (2011). On the other hand, the computational time decreases as Δ increases (Fig. 7b), and the time T (s) required to complete the simulation with Δ = 20 m is about 2.5 times lower than with Δ = 15 m. Accordingly, the 20 m grid has been selected as a reference for the following simulations.

Using the reference mesh Δ = 20, the sensitivity analysis on the roughness coefficient (in the range from 0.04 to 0.05 s m$^{-1/3}$) shows that the lower is the roughness coefficient, the higher is the peak discharge and the faster is the flood wave propagation, although the differences are rather small (Fig. 8). In general, the shape of the hydrographs is not significantly affected by the roughness coefficient and their rising limb is slightly steeper than the experimental one. The roughness coefficient has also limited effects on the flood wave arrival time, since the difference between the arrival times predicted with n = 0.04 s m$^{-1/3}$ and n = 0.05 s m$^{-1/3}$ is 80 s, that

corresponds to 11% of the measured wave travel time from Section 23 to Cepina. Focusing on the peak discharge, the maximum difference between the simulations with different roughness is about 245 $m^3 s^{-1}$ (i.e., 2.5% of the measured value). Finally, it has been verified that the roughness coefficient does not significantly affect the extent of the flooded area.

The match between the observed and numerical hydrographs computed using different values of the Manning's coefficient can be quantified by global performance indexes, as the Nash-Sutcliffe efficiency index (*NSE*; Nash and Sutcliffe, 1970) and the root mean square error (*RMSE*). Table 2 shows that the simulation performed with $n = 0.05$ s $m^{-1/3}$ provides the best overall performance. On the other hand, if the analysis is focused on the peak discharge and on the dam-break wave arrival time, the best agreement is obtained with $n = 0.045$ s $m^{-1/3}$. This simulation perfectly matches the arrival time and slightly underestimates (difference of 190 $m^3 s^{-1}$) the peak discharge at Cepina. Accordingly, in the following the coefficient $n = 0.045$ s $m^{-1/3}$ is used as reference value. Finally, the flood inundation map reported in Fig. 9 compares experimental and numerical flood extents for the valley stretch from Section 23 to Cepina. The flooded area computed with HEC-RAS 2D ($\Delta = 20$ m and $n = 0.045$ s $m^{-1/3}$) is in very good agreement with the observed one as confirmed also by the dimensionless performance index *P* (Horritt and Bates, 2002):

$$P = \frac{A_{sim} \cap A_{obs}}{A_{sim} \cup A_{obs}}$$

which theoretically ranges between 0 (no overlap) and 1 (complete overlap), and is equal to 0.75.

Comparison with the results of TELEMAC 2D and discussion

The capability of HEC-RAS 2D to cope with the propagation of dam-break waves is compared in this section with the freeware solver TELEMAC 2D which is widely used in engineering practice for dam-break modeling and was already tested with the Malpasset dam-break accident (Hervouet and Petitjean, 1999). TELEMAC 2D is commonly used in dam-break studies, even in the presence of sediment transport (e.g., El Kadi Abderrezzak et al., 2014), and in studies concerning the sudden waves generation and propagation of rapidly varied unsteady flows (Alho and Aaltonen, 2008).

The computational mesh used in the TELEMAC 2D model was built by interpolating the underlying DTM_Sect23_Cepina on unstructured triangular elements with sizes varying from 10 m (along the channel) up to 100 m (in the areas more distant from the stream) through a classic inverse distance method. A computational efficiency analysis showed that reducing the mesh size up to a factor 4 increases significantly the computational time without influencing the peak discharge and the flood wave arrival time at Cepina. Only the results obtained using n = 0.045 s $m^{-1/3}$ are compared in the following. The same upstream boundary condition used in HEC-RAS 2D was prescribed in TELEMAC 2D. A far-field condition was imposed along the downstream end of the computational domain as customary done in similar situations (e.g., Wang et al., 2011). A finite element approximation coupled with the conservative N-scheme (Roe, 1987; Hervouet et al., 2011), suitable for initially dry domains, was adopted. The parameters set suggested in the TELEMAC 2D validation manual (Mattic, 2018) for the Malpasset dam-break test case was adopted. Finally, a fixed time step equal to 0.1 s was chosen to guarantee a good compromise between numerical stability and computational efficiency.

The discharge hydrograph predicted by TELEMAC 2D at Cepina closely matches both the numerical hydrograph obtained with HEC-RAS 2D and the experimental one in terms of shape, peak discharge, and flood wave arrival time (see Tab. 3 and Fig. 10). The comparison between numerical results and experimental data shows that TELEMAC 2D overestimates the arrival time of the flood wave of approximately 20 s and underestimates the peak discharge of about 525 m^3 s^{-1}. HEC-RAS 2D better predicts the arrival time and the peak discharge; on the other hand, TELEMAC 2D better matches the recession limb (Fig. 10) of the hydrograph, slightly improving the values of *NSE* and *RMSE* (see Tabs. 2 and 3).

Compared to the measured flood extent, the performance of TELEMAC 2D is very similar to the one provided by HEC-RAS 2D (P = 0.75). The comparison between the flooding extent predicted by the two numerical models leads to P=0.82, which could suggest that the small discrepancies between numerical results and experimental data are due to the non-perfect reconstruction of the original topography of the laboratory model.

The comparisons presented so far confirm the capability of HEC-RAS 2D to deal with dam-break flood propagation in moderately steep alpine valleys, but they do not provide evidence about the capability of modeling dam-break flows in steep valleys with very irregular bathymetry. Accordingly, a comparative

simulation with HEC-RAS 2D and TELEMAC 2D was performed on the upper part of the valley using the bathymetry provided by DTM_dam_Sect23. Considering the natural irregularity of the crooked and steep valley upstream of Section 23, the coefficient $n = 0.05$ s m$^{-1/3}$ was used (e.g., Chow, 1959). The measured hydrograph at the dam (dark blue line in Fig. 5) coupled with a bed slope of 0.078 m/m, was used as upstream boundary condition. A normal depth downstream boundary condition and a dry bed initial condition were assumed.

The discharge hydrographs predicted by HEC-RAS 2D (on a computational grid with $\Delta = 20$ m) and TELEMAC 2D at Section 23 (Fig. 11) are very similar and show an overall good agreement also with the experimental one, as confirmed by the values of *NSE* and *RMSE* reported in Tab. 4. Both models accurately reproduce the measured peak discharge, even if they have a slightly steeper rising limb and a milder recession limb than the observed one. The most noticeable difference between the experimental and numerical hydrographs is the overestimation of approximately 140 s of the arrival time at Section 23.

A sensitivity analysis was performed for this additional test case in order to assess the influence of the roughness coefficient (ranging in the interval previously mentioned) on flood wave arrival time and peak discharge. It was observed that the peak discharge is slightly influenced (approximately 4% of the measured peak discharge) and the arrival time is practically not affected by the roughness coefficient.

In the authors' opinion, the violation of the SWE hypothesis of small bed slopes in the upper reach of the valley cannot justify the observed discrepancy between the arrival time of the measured and computed hydrographs. On the other hand, this stretch of the valley did not suffer relevant changes in the last century since the steepness of the slopes did not allow urban development, and the construction of transversal structures as well as the effects of scour and deposition did not change the thalweg of the valley to the point of being effective on the propagation of a dam break wave that is order of magnitudes larger than natural extreme floods. The differences can't be explained by the neglected role of vegetation, floating debris, and sediment transport either, considering that the term of comparison is a hydrograph measured in a physical model where all these components were totally disregarded. We eventually believe that the observed differences between measured and simulated hydrographs can be more probably explained by differences between DTM_dam_Sect23 and the actual geometry of the physical model which, as mentioned above, was probably based on poorly detailed topographic maps. However, the observed dissimilarities seem negligible if the modeling purpose is the assessment of flood hazard due to a dam-break event. In the authors' opinion, the good overall agreement

between the measured and simulated hydrographs demonstrates the practical validity of the SWE approximation even in situations where their theoretical limits are exceeded.

Conclusions

The paper by De Marchi (1945) concerning the hypothetical collapse of the Cancano I dam provides an extraordinary example of coupling between physical and numerical models to study the propagation of a dam-break wave along a very steep and irregular alpine valley and in the following floodplain. The knowledge of this valuable work was so far almost restricted to Italian scholars only. In the present paper, some of the data underlying the historical analysis were reconstructed, and a reliable test case (including topography and measured hydrographs) is presented concerning the dam-break wave propagation along the 7 km stretch between Section 23 and Cepina, for the total collapse scenario. An additional test case, more interesting in view of the significant valley steepness and ruggedness but less accurate because of the partial uncertainties on the original bathymetry, was also provided for the 8 km long stretch between the dam and Section 23. Despite this limitation, the original measured discharge hydrographs, complemented with a suitably reconstructed bathymetry, constitute an almost unique data set for the validation of the numerical models. This data set is now made available to the scientific community as supplementary material to this paper.

Both the test cases were used to successfully test the capability of the recently released software HEC-RAS 2D to model the propagation of a dam-break wave in alpine area. In addition, the results obtained with HEC-RAS 2D were compared with the numerical predictions provided by the freeware software TELEMAC 2D, which is widely used for this kind of applications. The good match between the results obtained with the two software suggests that the small differences between the experimental data and the numerical results might be related to some deficiencies in the reproduction of the original bathymetry, especially in the upper part of the valley. In conclusion, HEC-RAS 2D proved to be able to accurately model the propagation of impulsive floods, even on very steep and rugged domains. The comparison between numerical and measured hydrographs confirmed that, in spite of their theoretical limitations, the 2D SWE provide invaluable information for flood hazard mapping, even in the presence of steep bathymetries.

Data Availability Statement

The data of the Cancano test case used during the study are available in an online repository of the Hydraulic Engineering Group Brescia website at the address http://hydraulics.unibs.it/hydraulics/4558-2/. The following data are made available:

- S1 – Readme file describing the structure of the uploaded files
- S2 – Copy of the Italian version of the original paper by De Marchi (1945)
- S3 – A virtual flight of the valley from the Cancano dam to Tirano
- S4 – DTM_dam_Sect23 – (Modified from an official DTM of Regione Lombardia)
- S5 – DTM_Sect23_Cepina – (Built by the Authors)
- S6 – Measured discharge hydrographs at the dam, at Section 23, and at Cepina for the total collapse scenario (Digitized from De Marchi, 1945)
- S7 – Shapefile with the location of the cross section of the dam, Section 23, and Cepina (Digitized from De Marchi, 1945)
- S8 – Shapefile with the measured flooded areas from Section 23 to Cepina for the total collapse scenario (Digitized from De Marchi, 1945)

Notation list

The following symbols are used in this paper:

A_{sim} = computed flooded area;

A_{obs} = measured flooded area

n = Manning's coefficient;

NSE = Nash-Sutcliffe efficiency index;

P = performance index;

Q = flow discharge;

Q_p = peak flow discharge;

RMSE = root mean square error;

R = Reynolds number

R* = friction Reynolds number$t$ = time variable;

T = computational time;

t_a = flood wave arrival time;

u^* = shear velocity;

Δ = average computational cell size;

ε = roughness scale length;

423 v = kinematic viscosity.

424

425 **References**

426 Afshari, S., Tavakoly, A. A., Rajib, M. A., Zheng, X., Follum, M. L., Omranian, E., and Fekete, B. M. (2018).
427 "Comparison of new generation low-complexity flood inundation mapping tools with a hydrodynamic model."
428 *J. Hydrol*, 556, 539–556.

429 Alho, P., and Aaltonen, J. (2008). "Comparing a 1D hydraulic model with a 2D hydraulic model for the
430 simulation of extreme glacial outburst floods." *Hydrol. Process.*, 22(10), 1537-1547.

431 Alcrudo, F., and Mulet, J. (2007). "Description of the Tous dam-break case study (Spain)." *J. Hydraul. Res.*,
432 45(Extra Issue), 45–57.

433 Aureli, F., Maranzoni, A., Mignosa, P., and Ziveri, C. (2008). "Dam-break flows: acquisition of experimental
434 data through an imaging technique and 2D numerical modeling." *J. Hydraul. Eng.*, 134(8), 1089-11.

435 Bates, P.D., and Hervouet, J.M. (1999). "A new method for moving-boundary hydrodynamic problems in
436 shallow water." *Proc. of the Royal Society. Series A- Mathematical Physical and Engineering Sciences*, Vol.
437 455.

438 Begnudelli, L., and Sanders, B. F. (2007). "Simulation of the St. Francis dam-break flood." *J. Eng. Mech.*,
439 133(11), 1200–1212.

440 Bermudez, A., and Vazquez, E. (1994). "Upwind methods for hyperbolic conservation-laws with source
441 terms." *Comput. Fluid.*, 23(8), 1049-1071.

442 Bradford, S.F., and Sanders, B.F. (2002). "Finite-volume model for shallow-water flooding of arbitrary
443 topography." *J. Hydraul. Eng.*, 128(3), 289-298.

444 Brufau, P., Vázquez-Cendón, M.E., and García-Navarro, P. (2002). "A numerical model for the flooding and
445 drying of irregular domains." *Int. J. Numer. Meth. Fl.*, 39(3), 247-275.

446 Brunner, G. W. (2016). "HEC-RAS River analysis systems user's manual. Version 5.0." *U.S. Army Corps of*
447 *Engineers Institute for Water Resources Hydrologic Engineering Center*, Davis (CA).

448 Brunner, G. W. (2018a). "Benchmarking of the HEC-RAS Two-Dimensional Hydraulic Modeling
449 Capabilities." *U.S. Army Corps of Engineers Institute for Water Resources Hydrologic Engineering Center*,
450 Davis (CA).

Brunner, G. W. (2018b). "Verification and Validation Tests." *U.S. Army Corps of Engineers Institute for Water Resources Hydrologic Engineering Center*, Davis (CA).

Caleffi, V., Valiani, A., and Zanni, A. (2003). "Finite volume method for simulating extreme flood events in natural channels," *J. Hydraul. Res.*, 41(2), 167-177.

Casulli, V., and Stelling, G. S. (2011). "Semi- implicit subgrid modelling of three- dimensional free- surface flows." *Int. J. Numer. Meth. Fluids*, 67, 441-449.

Chanson, H. (2004). *The Hydraulics of Open Channel Flows, An Introduction*, 2nd Edition, Elsevier, Oxford, U.K..

Chaudhry M.H., (2008). *Open-Channel Flow*, 2nd Edition, Springer, U.S.

Chaudhry, M.H., Mercer, A.G., and Cass, D.E. (1983). "Modeling of slide-generated waves." *J. Hydraul. Eng.*, 109(11), 1505-1520.

Chow, V. T. (1959). *Open-channel hydraulics*, McGraw-Hill civil engineering series, Tokyo.

Cunge, J. A., Holly, F. M., Jr., and Verwey, A. (1980). *Practical aspects of computational river hydraulics*, Pitman Publishing, London.

Defina, A. (2000), "Two-dimensional shallow flow equations for partially dry areas." *Water Resour. Res.*, 36(11), 3251-3264

Delestre, O., Lucas, C., Ksinant, P. A., Darboux, F., Laguerre, C., Vo, T. N. T., James, F., and Cordier, S. (2013). "SWASHES: a compilation of shallow water analytic solutions for hydraulic and environmental studies." *Int. J. Num. Meth. Fluids*, 72(3), 269–300.

De Marchi, G. (1945). "Sull'onda di piena che seguirebbe al crollo della diga di Cancano. [On the dam-break wave resulting from the collapse of the Cancano dam]." *L'Energia Elettrica*, 22, 319–340 (in Italian).

D'Oria, M., Maranzoni, A., and Mazzoleni, M. (2019). "Probabilistic assessment of flood hazard due to levee breaches using fragility functions." *Water Resour. Res.*, 55.

El Kadi Abderrezzak, K., Ata, R., Tassi, P., Wang, D., Hervouet, J-M, and DieMoran, A. (2014). "2-D and 3-D numerical modeling of dam break waves over moveable beds." *Proc., 11th International Conference on Hydroinformatics*, New York, USA.

Erpicum, S., Archambeau, P., Dewals, B., Detrembleur, S., Fraikin, C. and Pirotton, M. (2004). “Computation of the Malpasset dam break with a 2D conservative flow solver on a multiblock structured grid.” *Proc., 6th International Conference on Hydroinformatics*, Singapore, China.

Fraccarollo, L., and Toro, E. F. (1995). "Experimental and numerical assessment of shallow water model for two-dimensional dambreak type problems." *J. Hydraul. Res.*, 33, 843-864.

Goutal, N. (1999). “The Malpasset dam failure. An overview and test case definition.” *Proc., of the 4th CADAM meeting*, University of Zaragoza, Spain.

Henderson, F.M. (1966). *Open channel flows*, Macmillan, New York, U.S.A.

Hervouet, J. M., and Petitjean, A. (1999). “Malpasset dam-break revisited with two-dimensional computation.” *J. Hydraul. Res.*, 37(6), 777–788.

Hervouet, J.-M., Razafindrakoto, E., and Villaret, C. (2011). “Dealing with dry zones in free surface flows: a new class of advection schemes.” *Proc., 34th IAHR World Congress: 33rd Hydrology and Water Resources Symposium and 10th Conference on Hydraulics in Water engineering: balance and uncertainty – water in a changing world*, Engineers Australia, Brisbane.

Horritt, M.S., and Bates, P.D. (2002). “Evaluation of 1D and 2D numerical models for predicting river flood inundation.” *J. Hydrol.*, 268(1-4), 87-99.

Hou, J., Liang, Q., Simons, F., and Hinkelmann, R. (2013). “A 2D well-balanced shallow flow model for unstructured grids with novel slope source term treatment”. *Adv. Water Resour.*, 52, 107–131.

ICOLD (1998). “Dam-break flood analysis—Review and recommendations.” Bulletin 111.

Jarrett, R. D. (1984) “Hydraulics of high gradient streams.” *J. Hydraul. Eng.*, 110(11), 1519–1539.

Jarrett, R.D., and Costa, J.E. (1986). “Hydrology, geomorphology, and dam-break modeling of the July 15, 1982, Lawn Lake Dam and Cascade Lake Dam failures, Larimer County, Colorado”. US Government Printing Office, Washington, USA.

MacDonald, I., Baines, M.J., and Nichols, N.K. (1997) “Analytic benchmark solutions for open-channel flows.” *J. Hydraul. Eng.*, 123(11), 1041-1045.

Martínez-Aranda, S., Fernández-Pato, J., Caviedes-Voullième, D., García-Palacín, I., and García-Navarro, P. (2018). “Towards transient experimental water surfaces: A new benchmark dataset for 2D shallow water solvers.” *Adv. Water Resour.*, 121, 130–149.

505 Mattic, O. (2018). *Telemac2d - Validation Manual*. Version v7p3.
506 Milanesi L., and Pilotti, M. (2019). "A conceptual model of vehicles stability in flood flows." *J. Hydraul. Res.*,
507 in press.
508 Milanesi L., Pilotti M., Belleri A., Marini A., and Fuchs S. (2018). "Vulnerability to flash floods: a simplified
509 structural model for masonry buildings." *Water Resour. Res, 54(10),* 7177-7197.
510 Milanesi, L., Pilotti, M., and Ranzi, R. (2015). "A conceptual model of people's vulnerability to floods." *Water*
511 *Resour. Res., 51(1),* 182–197.
512 Milanesi L., Pilotti M. & Bacchi B. (2016). "Using web-based observations to identify thresholds of a person's
513 stability in a flow", *Water Resour. Res, 52(10),* 7793-7805.
514 Molinaro, P., and Natale, L. (1994). "Modelling of flood propagation over initially dry areas." *Proc., Specialty*
515 *Conference,* ASCE, New York.
516 Morris, M. (2000). "CADAM Concerted Action on Dambreak Modelling, Final report." HR Wallingford, UK
517 Morris, M. (2005). "IMPACT – Investigation of Extreme Flood Processes and Uncertainty, Final Technical
518 Report". IMPACT Project Reporting.
519 Nash, J. E., and Sutcliffe, J. V. (1970). "River flow forecasting through conceptual models part I — A
520 discussion of principles." *J. Hydrol.*, 10(3), 282–290.
521 Néelz, S., and Pender, G. (2013). "Benchmarking the Latest Generation of 2D Hydraulic Modelling Packages."
522 Report SC120002, DEFRA/Environment Agency, UK.
523 Paquier A., and Goutal N. (2016). "Dam and levee failures: an overview of flood wave propagation modelling."
524 *Houille Blanche,* 1, 5-12
525 Petaccia, G., Lai, C., Milazzo, C., and Natale, L. (2016). "The collapse of Sella Zerbino gravity dam." *Eng.*
526 *Geol.*, 211, 39-49.
527 Pianese, D., and Barbiero, L. (2004). Discussion of "Case study: Malpasset dam-break simulation using a two-
528 dimensional finite volume method." by Alessandro Valiani, Valerio Caleffi, and Andrea Zanni. *J. Hydraul.*
529 *Eng.*, 130(9), 941-944.
530 Pilotti, M. (2016). "Extraction of cross sections from digital elevation model for one-dimensional dam-break
531 wave propagation in mountain valleys." *Water Resour. Res.*, 52, 52-68.

Pilotti, M., Tomirotti, M., Valerio, G., and Bacchi, B. (2010). "Simplified method for the characterization of the hydrograph following a sudden partial dam break.", *J. Hydraul. Eng.*, 136(10), 693-704.

Pilotti, M., Maranzoni, A., Tomirotti, M., and Valerio, G. (2011). "1923 Gleno dam-break: case study and numerical modelling." *J. Hydraul. Eng.*,, 137(4), 480-492.

Pilotti, M., Maranzoni, A., Milanesi, L., Tomirotti M., and Valerio G. (2014). "Dam-break modeling in alpine valleys." *J. Mt. Sci.*, 11, 1429-1441

Quirogaa, V. M., Kurea, S., Udoa, K., and Manoa, A. (2016). "Application of 2D numerical simulation for the analysis of the February 2014 Bolivian Amazonia flood: application of the new HEC-RAS version 5." *Ribagua*, 3(1), 25–33.

Ritter, A. (1892). "Die fortplanzung der wasserwellen." *Vereine Deutcher Ingenieure Zeitswchrift*, 36, 947-954

Robb, D., and Vasquez, J. (2015). "Numerical simulation of dam-break flows using depth-averaged hydrodynamic and three-dimensional CFD models." *Proc., Canadian Society for Civil Engineering Hydrotechnical Conference*, Québec City.

Roe, P.L. (1987). "Linear advection schemes on triangular meshes. Technical report 8720." Cranfield Institute of Technology.

Savant, G., Berger, C., McAlpin, T.O., and Tate, J.N. (2011). "Efficient implicit finite-element hydrodynamic model for dam and levee breach." *J. Hydraul. Eng.*, 137(9), 1005-1018.

Shustikova, I., Domeneghetti, A., Neal, J. C., Bates, P., and Castellarin, A. (2019). "Comparing 2D capabilities of HEC-RAS and LISFLOOD-FP on complex topography." *Hydrological Sciences Journal*, 67(14), 1769-1782.

Soares Frazão, S., and Testa, G. (1999). "The Toce River test case: numerical results analysis." *Proc., 3rd CADAM workshop*, Milan.

Soares Frazão S., and Zech, Y. (2007). "Experimental study of dambreak flow against an isolated obstacle." *J. Hydraul. Res.*, 45(Special Issue), 27-36.

Soares Frazão, S., Morris, M. W., and Zech, Y. (2000). "Concerted action on dambreak modelling: Objectives, project report, test cases, meeting proceedings." Université Catholique de Louvain, Civ. Eng. Dept., Hydraulics Div., Louvain-la-Neuve, Belgium.

560 Soares Frazão, S., Zech, Y., and Morris, M. (2003). "IMPACT, Investigation of extreme flood processes and
561 uncertainty." Proc., 3rd IMPACT Project Workshop, Louvain-la-Neuve, Belgium
562 Stoker, J.J. (1948). "The formation of breakers and bores - the theory of nonlinear wave propagation in shallow
563 water and open channels." *Commun. Appl. Math.*, 1(1), 1-87
564 Su, S. T., and Barnes, H. (1970). "Geometric and frictional effects on sudden releases." *J. Hydraul. Div.*,
565 96(11), 2185–2200.
566 TELEMAC Modelling System (2011). *TELEMAC-2D, Version 6.1, Validation document*,
567 www.opentelemac.org.
568 Teng, J., Jakeman, A. J., Vaze, J., Croke, B. F., Dutta, D., and Kim, S. (2017). "Flood inundation modelling:
569 A review of methods, recent advances and uncertainty analysis." *Environ. Modell. Softw.*, 90, 201–216.
570 Testa, G., Zuccalà, D., Alcrudo, F., Mulet, J., and Soares Frazao, S. (2007). "Flash flood flow experiment in a
571 simplified urban district." *J. Hydraul. Res.*, 45(extra issue), 37–44.
572 Thacker, W.C. (1981). "Some exact-solutions to the non-linear shallow-water wave-equations." *J. Fluid.*
573 *Mech.*, 107(6), 499-508
574 Toro, E.F. (2001). *Shock-capturing Methods for Free-Surface Shallow Flows*, Wiley, Chichester, U.K..
575 Toro E.F., and Garcia-Navarro P. (2007). "Godunov–Type Methods for Free–Surface Shallow Flows: A
576 Review." *J. Hydraul. Res.*, 45(6), 736–751
577 Touma, R., and Kanbar, F. (2018). "Well-balanced central schemes for two-dimensional systems of shallow
578 water equations with wet and dry states." *Appl. Math. Modell.*, 62, 728–750.
579 Valiani, A., Caleffi, V., and Zanni, A. (2002). "Case study: Malpasset dam-break simulation using a two-
580 dimensional finite volume method." *J. Hydraul. Eng.*, 128(5), 460-472.
581 Wang, Y., Liang, Q., Kesserwani, G., and Hall, J.W. (2011). "A 2D shallow flow model for practical dam-
582 break simulations." *J. Hydraul. Res.*, 49(3), 307-316.
583 Yalin, M. S. (1977). *The mechanics of sediment transport*, Pergamon Press, Oxford, U.K.
584

Table 1. Peak discharges (Q_p) and wave arrival times (t_a) of the discharge hydrographs measured by De Marchi (1945) at three control cross-sections for the total and partial dam-break scenarios.

Control section	Total collapse		Partial collapse	
	Q_p (m^3 s^{-1})	t_a (s)	Q_p (m^3 s^{-1})	t_a (s)
Dam	50000	0	9314	0
Section23	18262	440	5745	580
Cepina	10161	1160	4299	1440

Table 2. Results of the sensitivity analysis on the roughness coefficient (reference mesh with 20 m average grid spacing).

Manning's n (s $m^{-1/3}$)	Q_p (m^3 s^{-1})	t_a (s)	*NSE* (-)	*RMSE* (m^3 s^{-1})
n = 0.040 s $m^{-1/3}$	10116	1120	0.82	1065
n = 0.045 s $m^{-1/3}$	9969	1160	0.92	703
n = 0.050 s $m^{-1/3}$	9871	1200	0.97	434

Table 3. Numerical results obtained with TELEMAC 2D (n = 0.045 s $m^{-1/3}$) for the discharge hydrograph at Cepina.

Q_p (m^3 s^{-1})	t_a (s)	*NSE* (-)	*RMSE* (m^3 s^{-1})
9637	1180	0.96	492

Table 4. Results of the numerical simulation of the flood wave propagation between the dam and Section 23 for the total collapse scenario.

HEC-RAS 2D				TELEMAC 2D			
Q_p (m^3 s^{-1})	t_a (s)	*NSE* (-)	*RMSE* (m^3 s^{-1})	Q_p (m^3 s^{-1})	t_a (s)	*NSE* (-)	*RMSE* (m^3 s^{-1})
18416	580	0.83	2336	18150	574	0.84	2274

Figure 1

Click here to access/download;Figure;Fig_1_REV.tiff

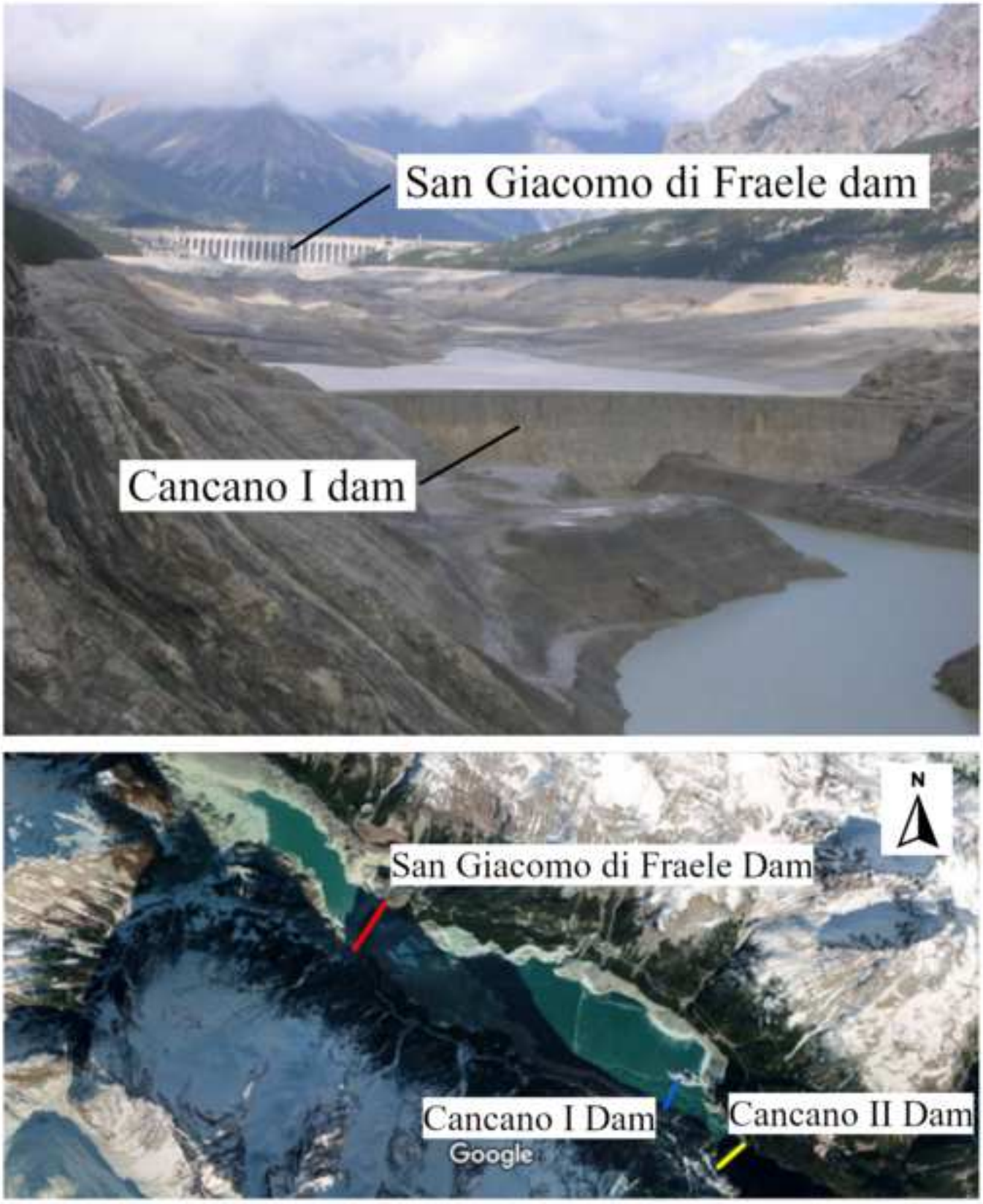

Figure 2

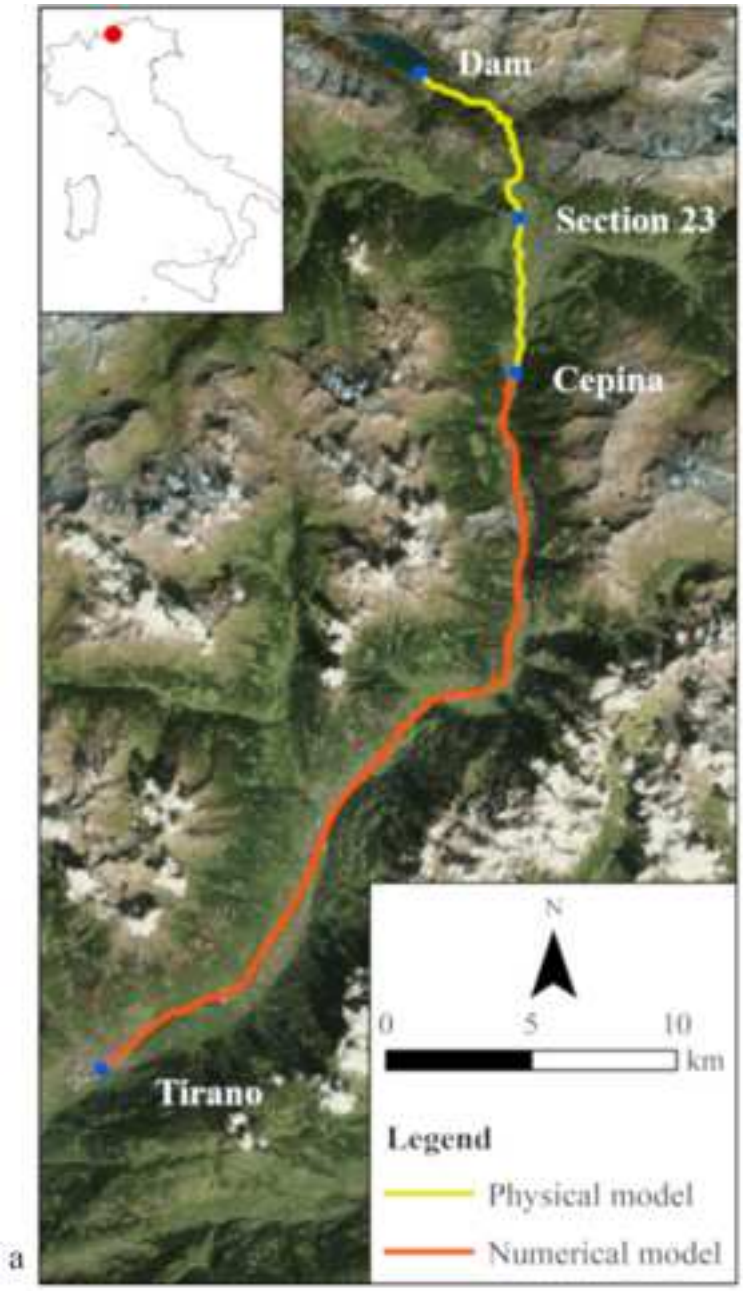

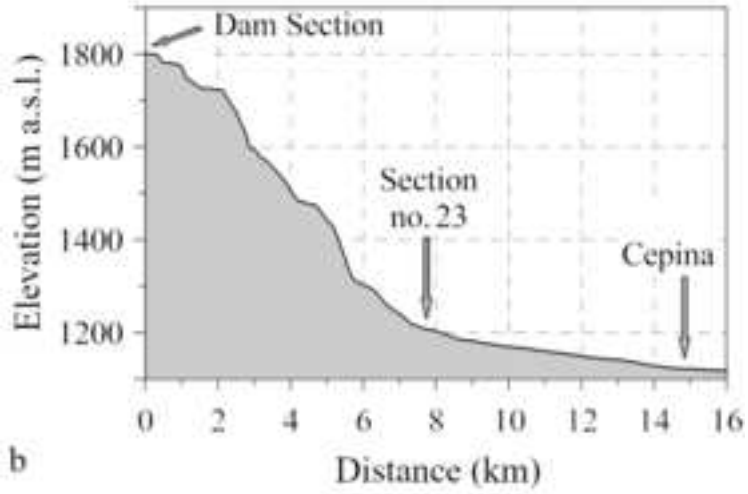

Figure 4

Click here to access/download;Figure;Fig_4_REV.tif

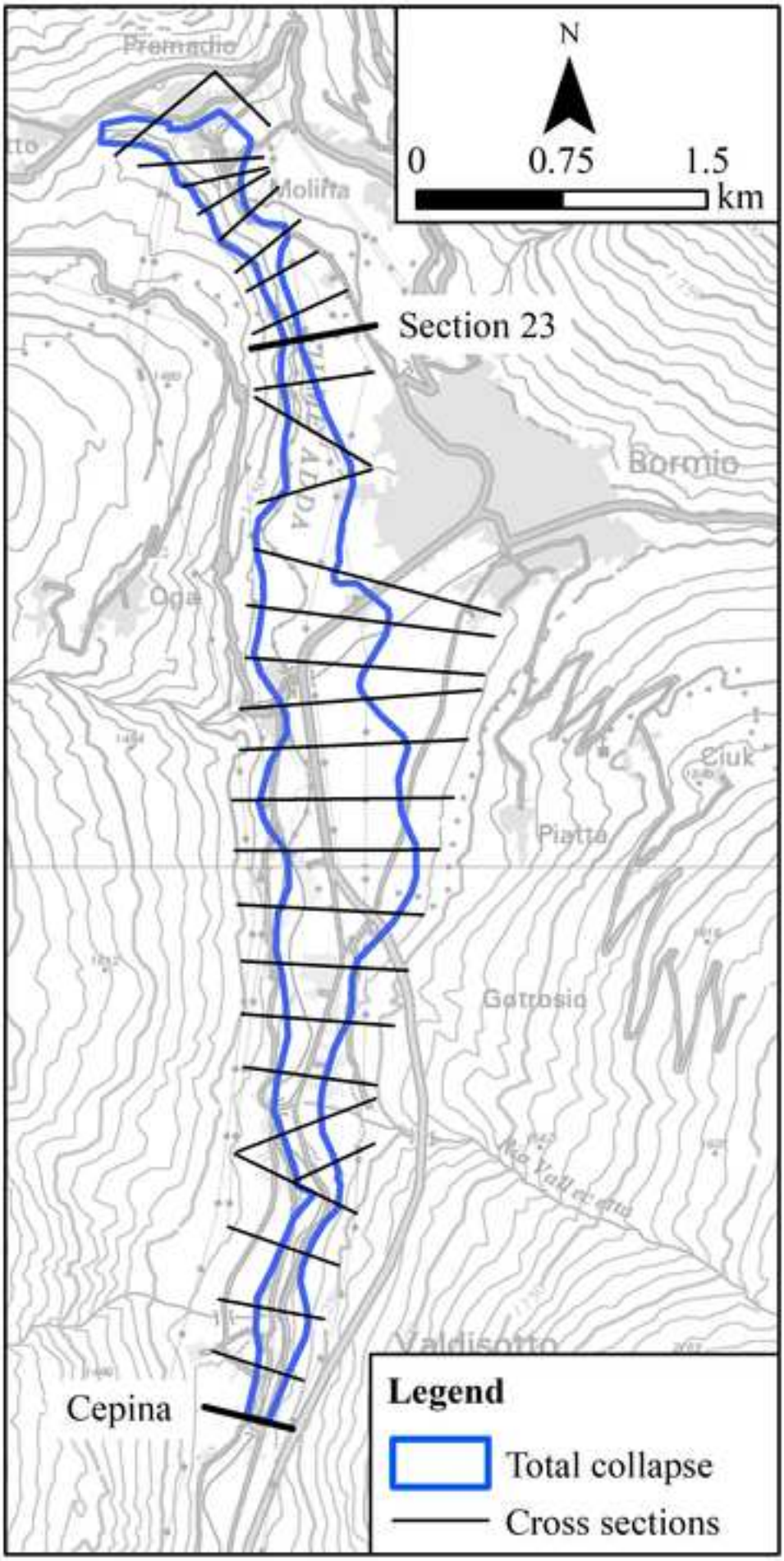

Figure 5

Click here to access/download;Figure;Fig_5_REV.tif

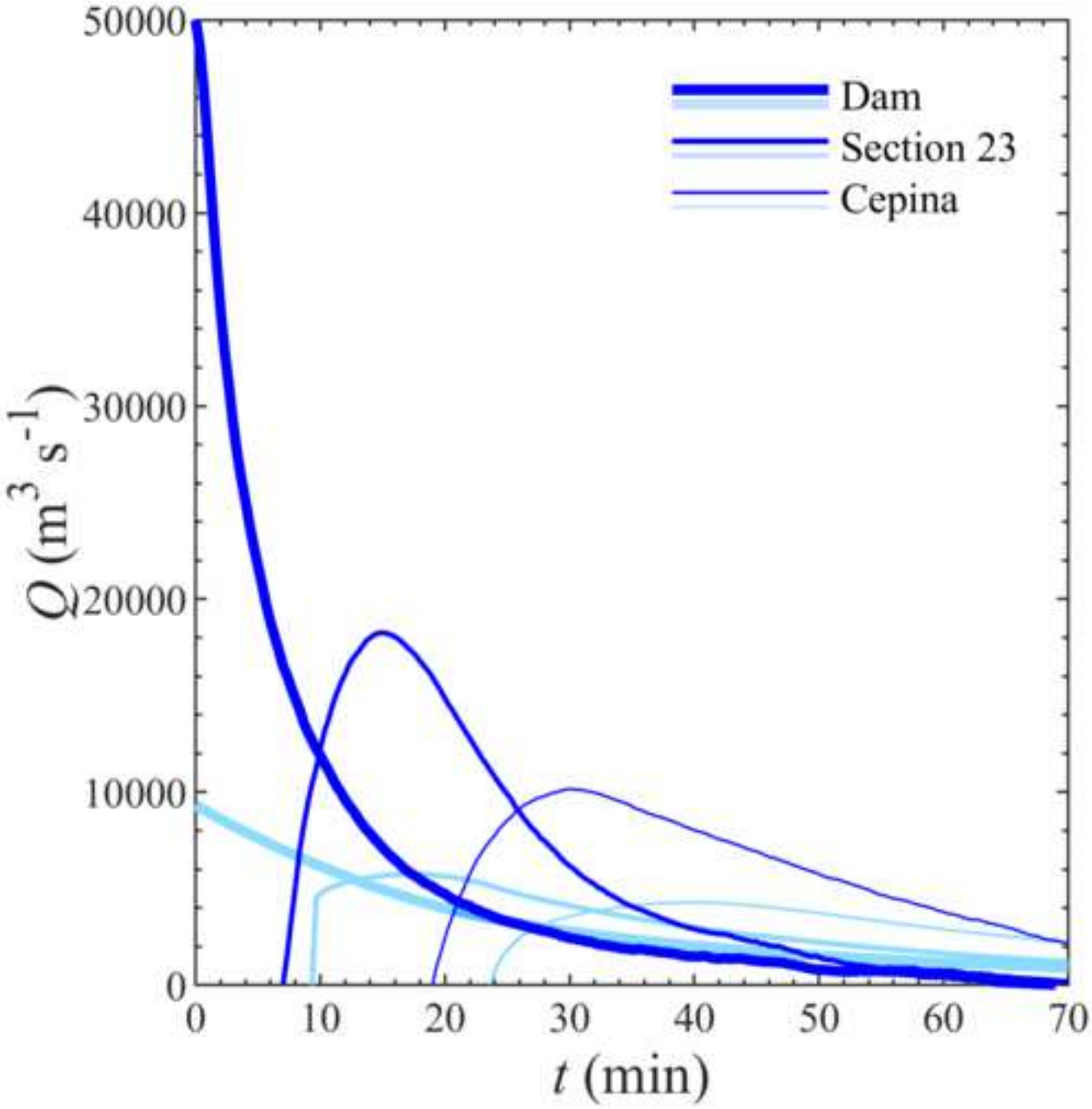

Figure 6

Click here to access/download;Figure;Fig_6_REV.tif

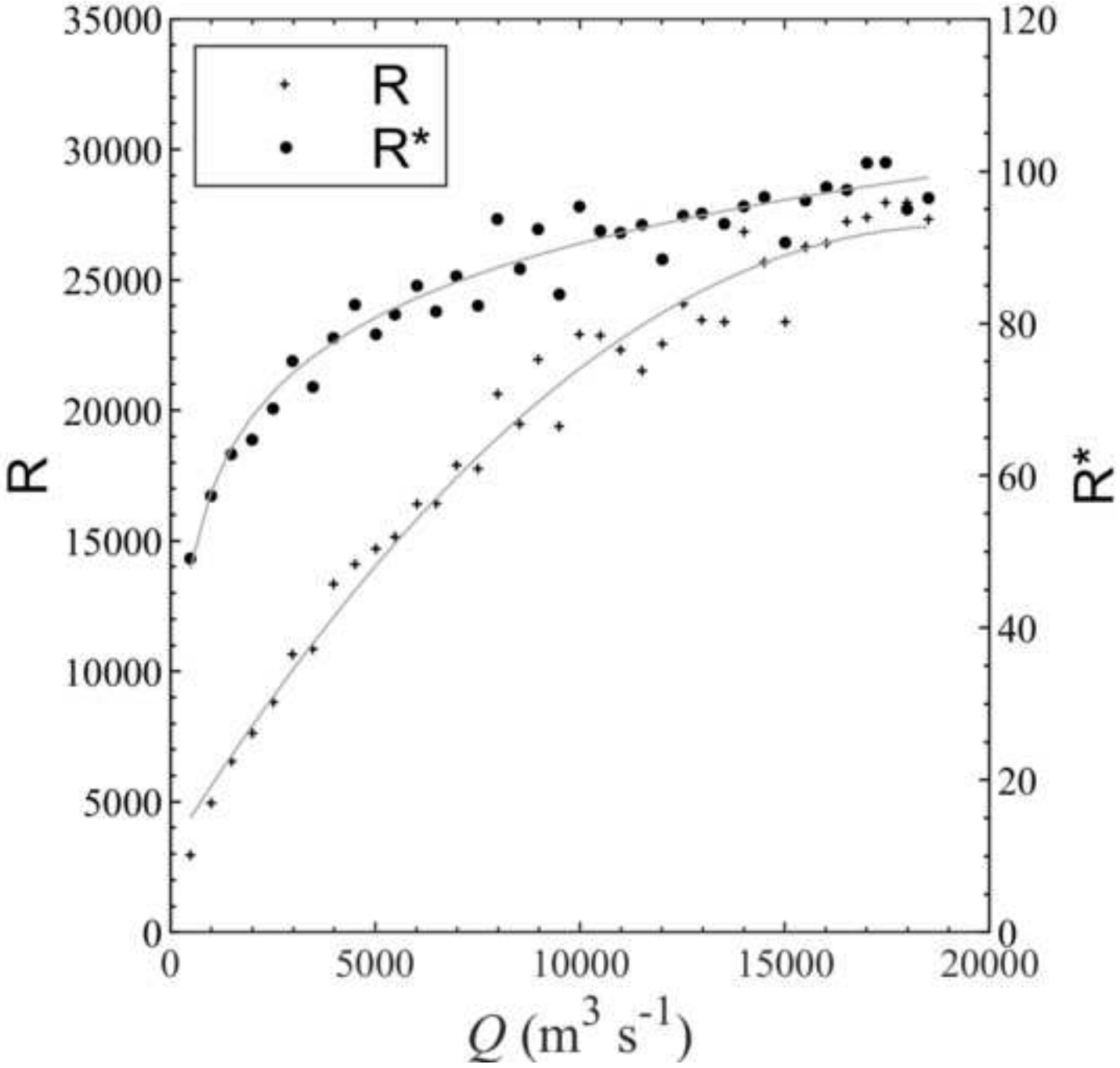

Figure 7

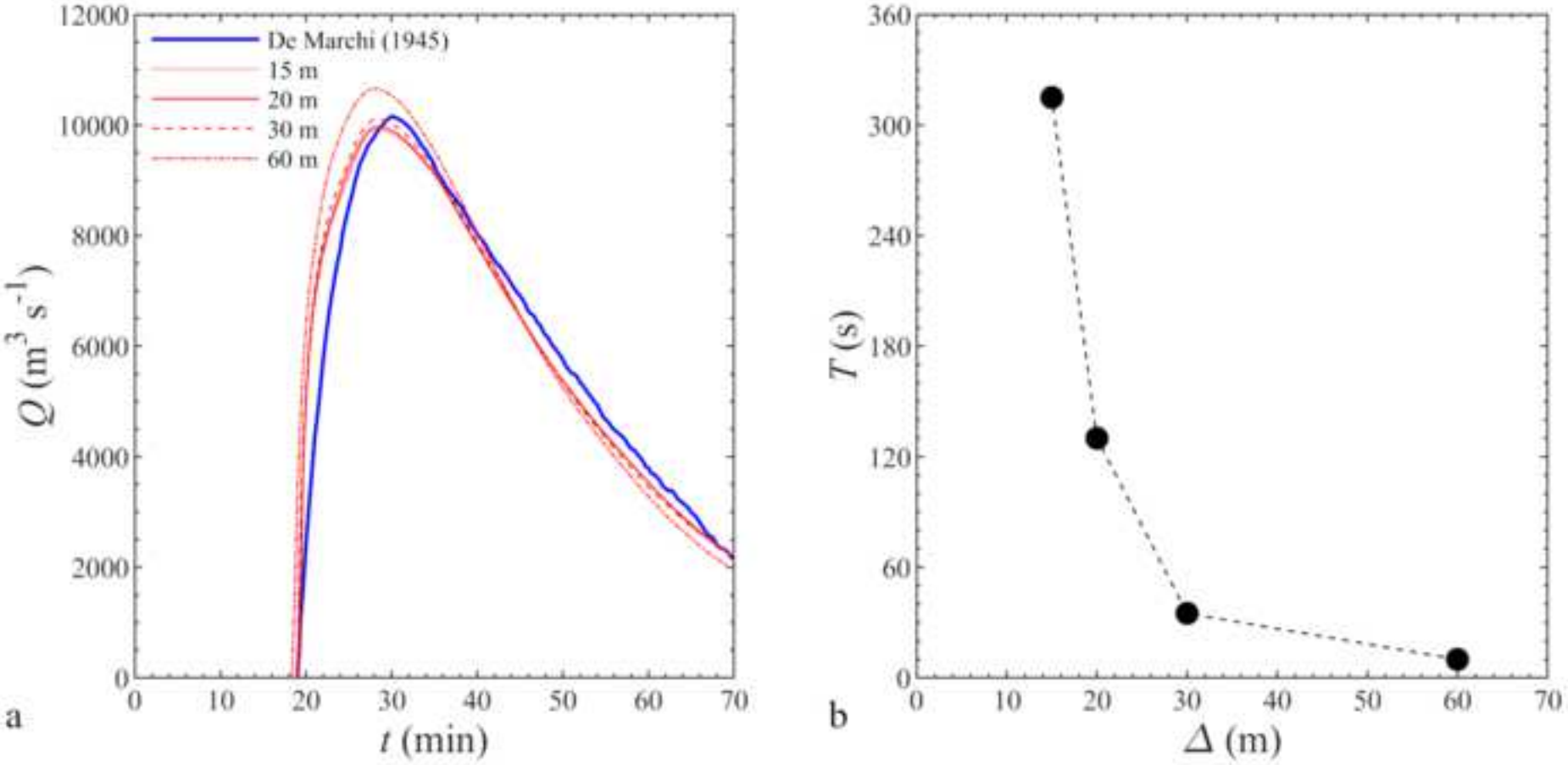

Figure 8

Click here to access/download;Figure;Fig_8_REV.tif

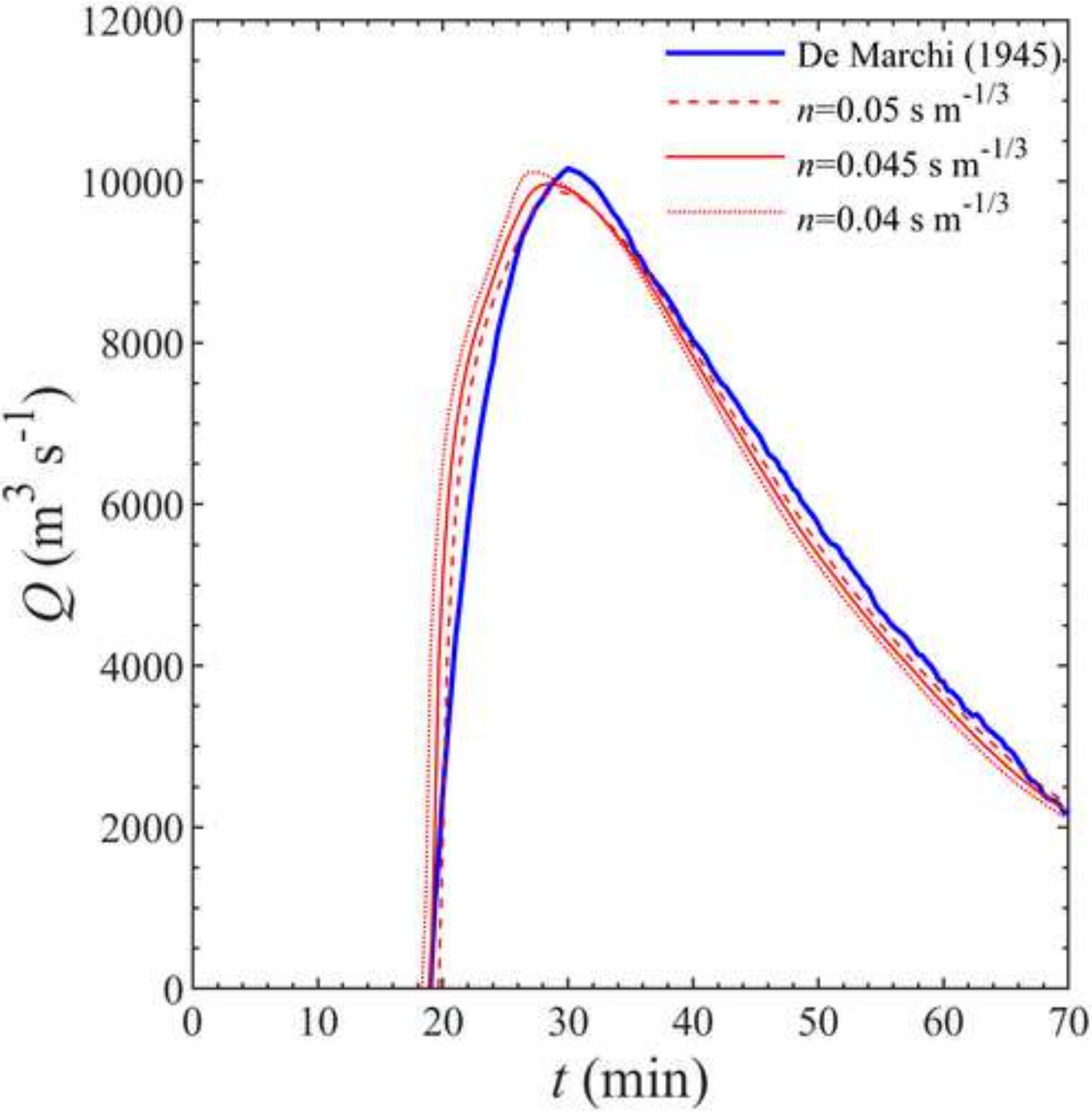

Figure 9

Click here to access/download;Figure;Fig_9_REV.tif

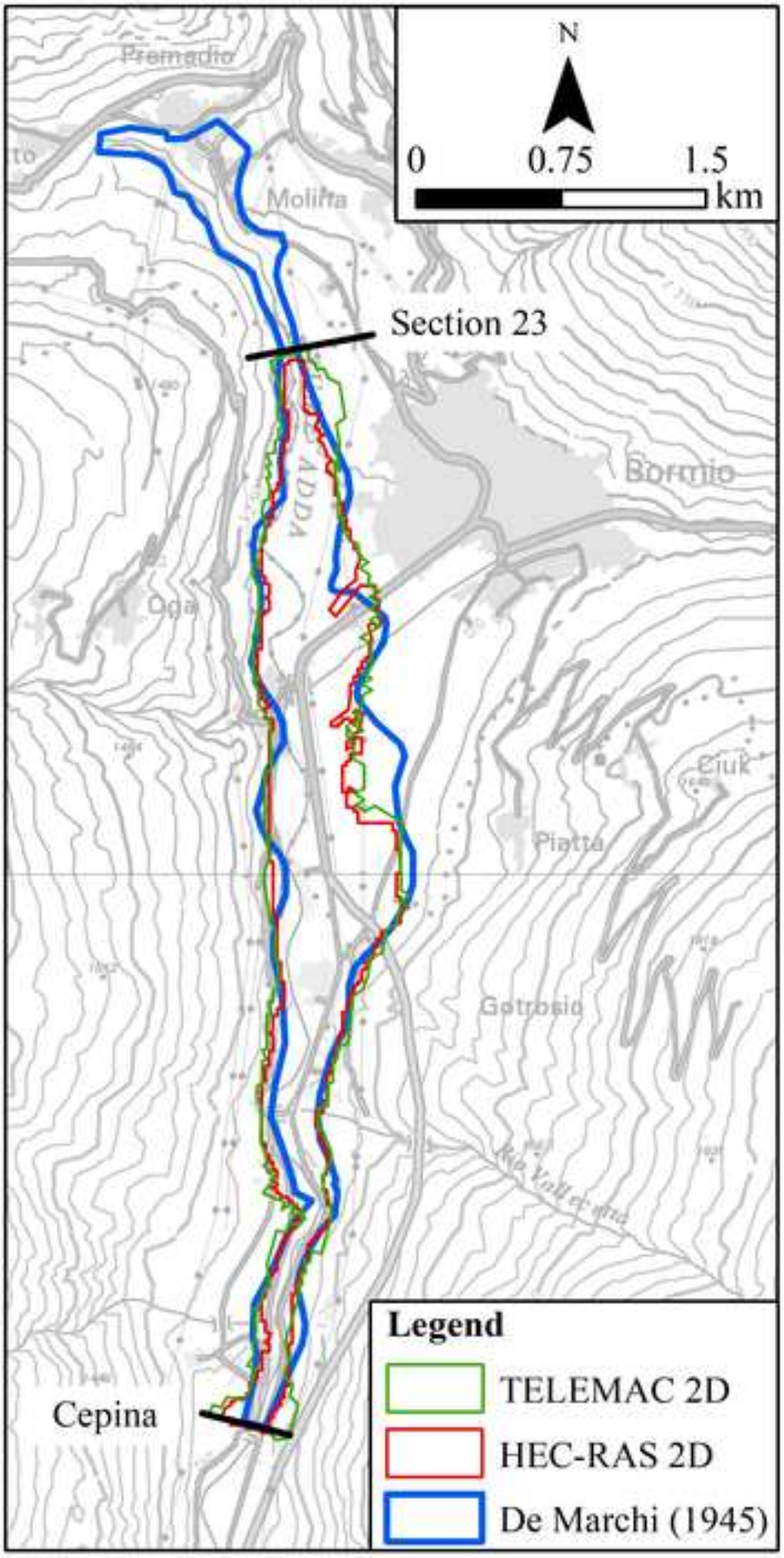

Figure 10

Click here to access/download;Figure;Fig_10_REV.tif

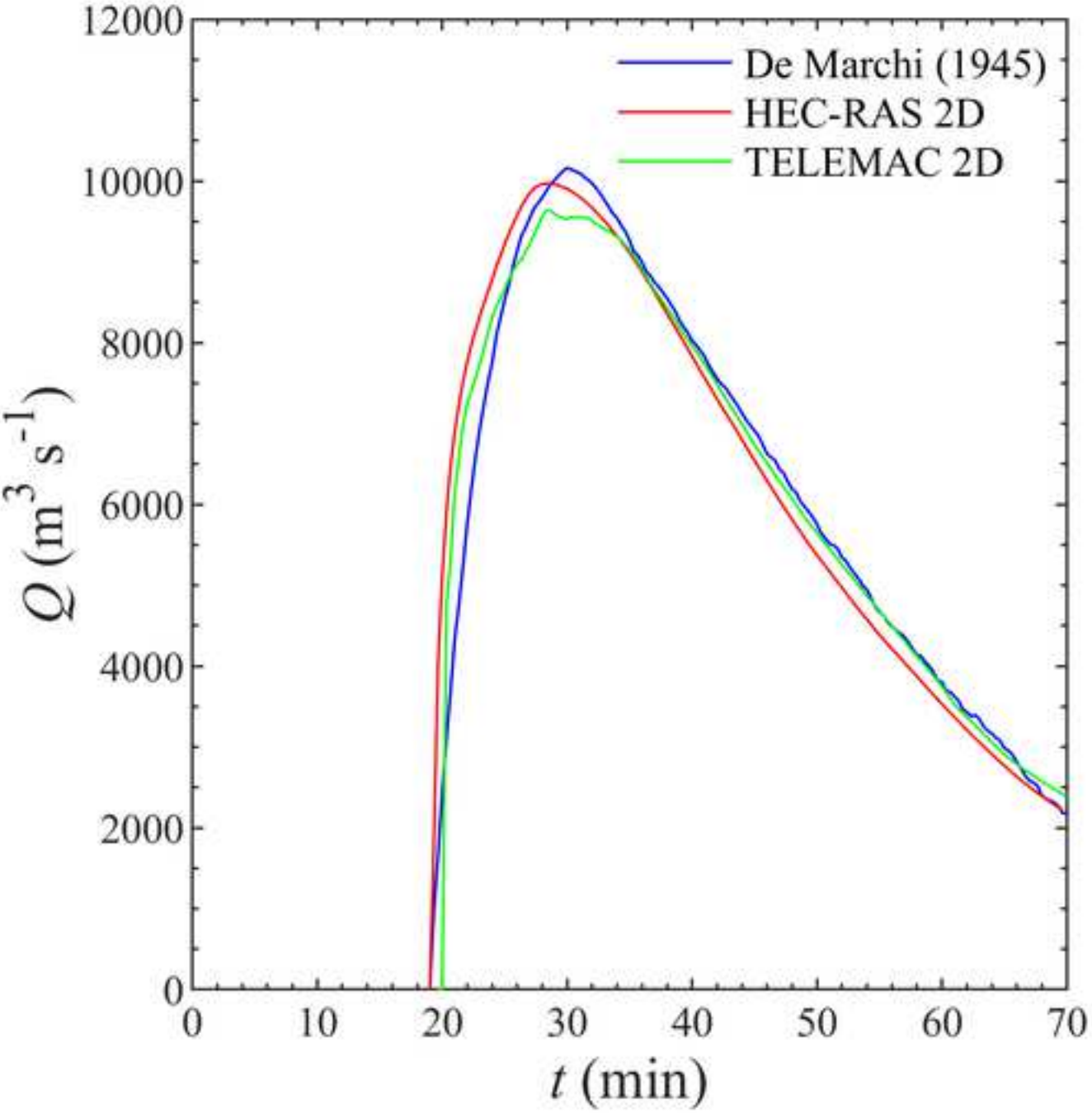

Figure 11

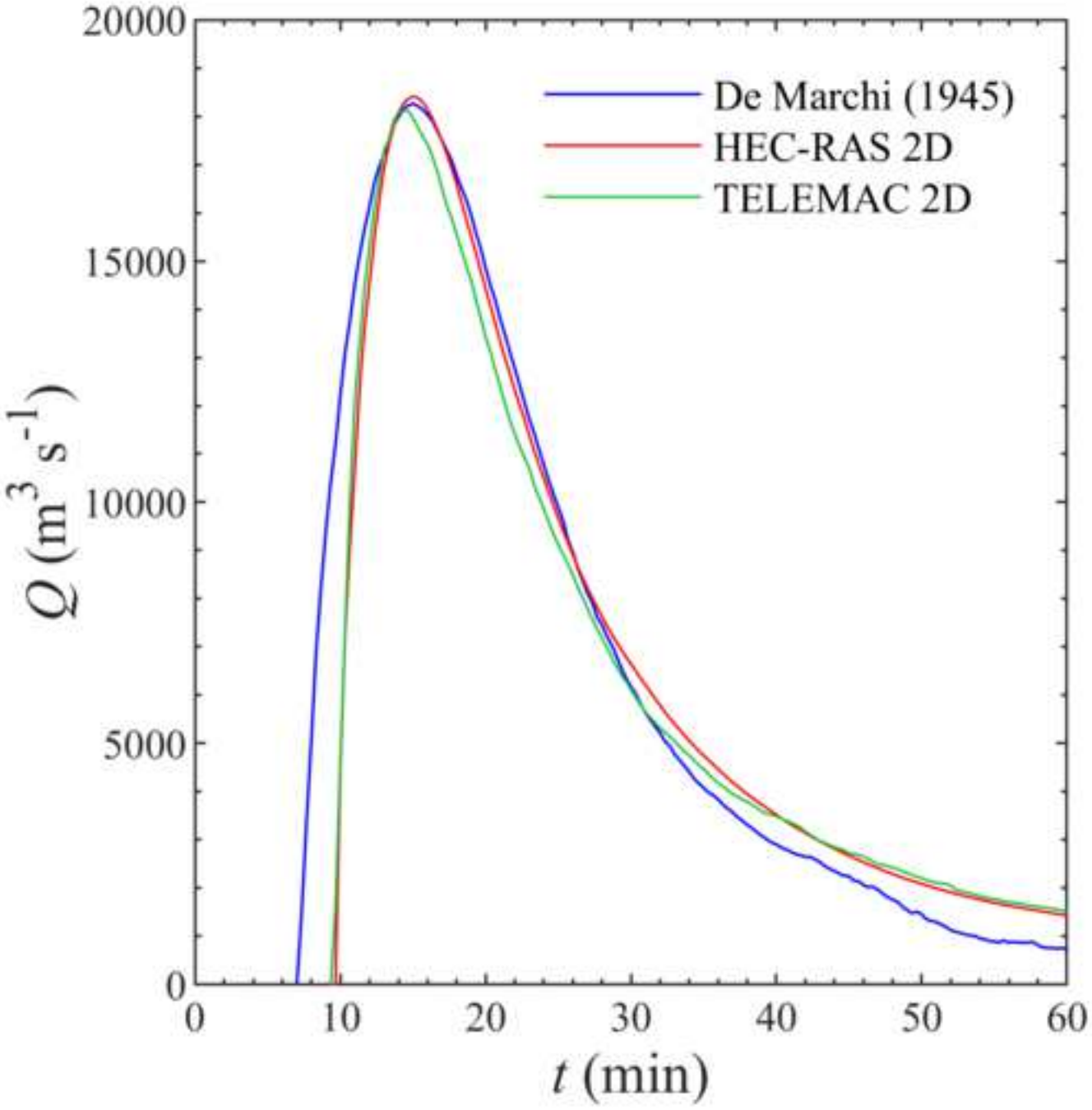

Figure captions

Fig. 1. (a) The Cancano I dam as seen from the Cancano II dam during a total emptying of the reservoir (courtesy of www.progettodighe.it). This reservoir is bounded upstream by the San Giacomo di Fraele dam. (b) Plan view of the current configuration of the San Giacomo and Cancano II dams with trace of the Cancano I dam.

Fig. 2. (a) Satellite view of the study area with the indication of the two stretches analyzed by De Marchi (1945) using physical and numerical models. The upper inset shows the location of the investigated site in the Italian Alps. (b) Longitudinal profile of the upstream stretch of the valley from the dam up to Cepina (modified from Pilotti et al., 2014).

Fig. 3. (a) Planimetric view of the physical model used by De Marchi to study the dam-break wave propagation between the dam and Cepina. The red dots show the locations of the discharge measurement stations. (b) View of the physical model: locations of the cross-sections used to reconstruct the valley bathymetry and recording instrument for measuring discharge hydrographs (modified from De Marchi, 1945).

Fig. 4. Flooded areas measured on the physical model for the total dam-break scenario with the exact location of the original cross-sections (digitized from De Marchi, 1945).

Fig. 5. Measured discharge hydrographs for the total (dark blue lines) and partial (light blue lines) collapse scenarios at three control cross-sections (digitized from De Marchi, 1945).

Fig. 6. Average values R and R* at the model scale as a function of the prototype discharges for the stretch between Section 23 and Cepina along with approximating curves.

Fig. 7. (a) Sensitivity of the total collapse discharge hydrograph computed at Cepina and (b) of the computational time T (s) on the average size of the computational grid Δ (data referred to a i7-8550U CPU with 16 GB RAM). The roughness coefficient is $n = 0.045$ s m$^{-1/3}$. Time t (min) is measured from the dam collapse.

Fig. 8. Sensitivity of the discharge hydrograph at Cepina on the value of the roughness coefficient (reference mesh with 20 m average grid spacing).

Fig. 9. Comparison of the observed flooded areas (De Marchi, 1945) with those predicted by HEC-RAS 2D ($n = 0.045$ s m$^{-1/3}$, 20 m average grid spacing) and TELEMAC 2D between Section 23 and Cepina.

Fig. 10. Comparison between the experimental discharge hydrograph at Cepina and the numerical hydrographs computed with HEC-RAS 2D and TELEMAC 2D ($n = 0.045$ s m$^{-1/3}$).

Fig. 11. Total collapse simulation along the stretch from the Cancano I dam to Section 23 ($n = 0.05$ s m$^{-1/3}$). Comparison between experimental and numerical discharge hydrographs at Section 23.